AIP | Journal of Applied Physics

Ultrahigh strain-rate bending of copper nanopillars with laser-generated shock waves

H. A. Colorado, A. Navarro, S. V. Prikhodko, J. M. Yang, N. Ghoniem, and V. Gupta

Citation: Journal of Applied Physics **114**, 233510 (2013); doi: 10.1063/1.4851055
View online: http://dx.doi.org/10.1063/1.4851055
View Table of Contents: http://scitation.aip.org/content/aip/journal/jap/114/23?ver=pdfcov
Published by the AIP Publishing


Re-register for Table of Content Alerts

Create a profile.  Sign up today! 

[This article is copyrighted as indicated in the article. Reuse of AIP content is subject to the terms at: http://scitation.aip.org/termsconditions. Downloaded to] IP: 128.97.83.27 On: Fri, 10 Jan 2014 00:16:10

Ultrahigh strain-rate bending of copper nanopillars with laser-generated shock waves

H. A. Colorado,[1,2,a)] A. Navarro,[3] S. V. Prikhodko,[1] J. M. Yang,[1] N. Ghoniem,[1,3] and V. Gupta[1,3,a)]
[1]*Department of Materials Science and Engineering, University of California Los Angeles, Los Angeles, California 90095, USA*
[2]*Department of Mechanical Engineering, Universidad de Antioquia, Medellin, Colombia*
[3]*Department of Mechanical and Aerospace Engineering, University of California Los Angeles, Los Angeles, California 90095, USA*

(Received 8 September 2013; accepted 4 December 2013; published online 19 December 2013)

An experimental study to bend FIB-prepared cantilevered single crystal Cu nanopillars of several hundred nanometers in diameter and length at ultrahigh strain rate is presented. The deformation is induced by laser-generated stress waves, resulting in local strain rates exceeding $10^7\,s^{-1}$. Loading of nano-scale Cu structures at these extremely short loading times shows unique deformation characteristics. At a nominal stress value of 297 MPa, TEM examination along with selected area electron diffraction characterization revealed that twins within the unshocked Cu pillars interacted with dislocations that nucleated from free surfaces of the pillars to form new subgrain boundaries. MD simulation results were found to be consistent with the very low values of the stress required for dislocation activation and nucleation because of the extremely high surface area to volume ratio of the nanopillars. Specifically, simulations show that the stress required to nucleate dislocations at these ultrahigh strain rates is about one order of magnitude smaller than typical values required for homogeneous nucleation of dislocation loops in bulk copper single crystals under quasi-static conditions. © *2013 AIP Publishing LLC*. [http://dx.doi.org/10.1063/1.4851055]

I. INTRODUCTION

Engineering applications involving nuclear explosions, blast loading, laser fusion energy, and asteroid impacts, among others, have motivated research into High Energy Material physics where material behavior is sought under extreme conditions of pressure (10–200 GPa) and strain rates (10^6–$10^8\,s^{-1}$). Recent efforts have revealed new deformation mechanisms under such extreme conditions, which do not follow the conventional dislocation barrier-type models[1–7] that assume motion of pre-existing dislocations via thermal activation and phonon drag. For example, Kiritani and co-workers[8,9] found thin face-centered cubic (fcc) metal (Au and Cu) samples to be dislocation-free and composed of stacking-fault tetrahedra and nanoscale voids when subjected to tension and compression loads at high strain rates. Remington *et al.*[10] found that in fcc metals with low stacking fault energy (such as copper), shock compression initiated the twinning-slip transition and a new $\alpha \rightarrow \varepsilon$ (bcc to hcp) phase transformation in iron during plastic deformation at sub-nanosecond time scales. Large-scale molecular dynamics (MD) simulations carried out to explain these observations, for example, by Li and Ghoniem,[11] showed that in pure Cu, there is a transition from dislocation- to twinning-dominated deformation because dislocation barriers do not exist *a priori*, and the energy differential between these two deformation modes is rather small. Bringa *et al.*[12] performed simulations with pre-existing dislocation sources in the form of prismatic loops in shocked Cu single crystals. Their simulations indicate that once the transient pressure wave exceeds the threshold for either activating the source (~10 GPa) or homogeneous nucleation of dislocations (~30 GPa), the dislocation density relaxes by a factor of three resulting in the onset of three-dimensional plastic relaxation behind the shock front with the formation of a high density of dislocations and stacking faults.

With an aim to further explore such newer deformation mechanisms, the present research in our group focuses on a combination of laser-shock loading of nanostructures, followed by their transmission electron microscopy (TEM) examination, and modeling of the evolving structures through MD simulation. Specifically, focused-ion-beam (FIB)-prepared single crystal columns of Cu of several hundred nanometers in length and diameter are loaded with laser-generated stress waves of 16–20 ns duration resulting in material strain rates of $10^7\,s^{-1}$ that are two orders of magnitude higher than those previously studied. Atomic-scale mechanisms (defect formation or annihilation, dislocation movement, twinning, etc.) that allow the material to rearrange itself when subjected to extreme conditions are then uncovered by direct TEM examination of the shocked samples. Finally, the experimental observations are used to validate and refine MD simulations to model the new phenomenon. Recently, we reported results on shock compression of Cu nanopillar where the column axes were aligned with the wave propagation (compression) direction.[13] Here, we report results from experiments where the same pillars were loaded

a)Authors to whom correspondence should be addressed. Electronic addresses: hcoloradolopera@ucla.edu and vgupta@seas.ucla.edu. Tel./Fax.: +1-(310) 206-3166. Present address: UCLA—MAE, Department Engineering, IV Bldg. 420 Westwood Plaza, Los Angeles, California 90095, USA.

 © 2013 AIP Publishing LLC

[This article is copyrighted as indicated in the article. Reuse of AIP content is subject to the terms at: http://scitation.aip.org/termsconditions. Downloaded to] IP: 128.97.83.27 On: Fri, 10 Jan 2014 00:16:10

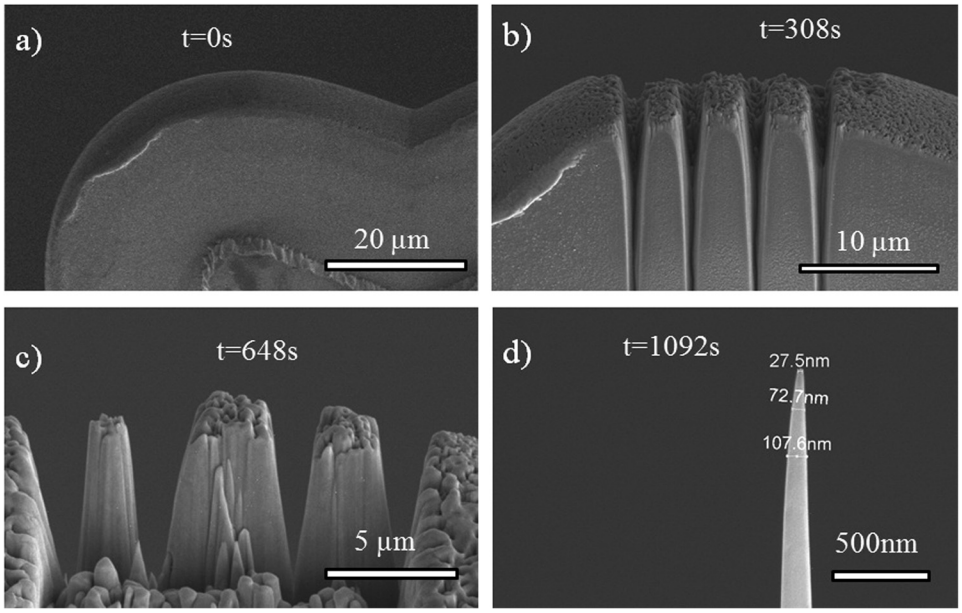

FIG. 1. Images show step-by-step procedure of the pillar structure fabrication on the tip of the TEM grid post using FIB.

by directing the stress wave transverse to the column axes. This resulted in dynamic bending of the pillars at nominal pressures and strain rates greater than 1 GPa and $10^7\,s^{-1}$, respectively. Barring minor changes, the same apparatus ,and test procedures as used in the axial compression study were used.[13] Deformation mechanisms were identified by TEM. MD simulations of shocked nano-pillars will be reported in a separate publication.

II. EXPERIMENTAL PROCEDURE

All experiments were carried out using single-crystal Cu(001) pillars in the Laser Spallation Facility, developed previously to measure the tensile strengths of interfaces.[14]

Copper nanopillars for this study were fabricated directly on the TEM grids purchased from Omniprobe AutoProbe™. As-received grids were annealed for 20 h at 150 °C to remove residual stresses. Nanopillars were then fabricated using the Nova 600 Dual Beam FIB/scanning electron microscope (SEM) system. Figure 1 shows the step-by-step procedure for fabricating the nanopillars at the tip of the Omniprobe grid post. Three pillars were made on each post, with a center-to-center separation of about 5 μm. All pillars were approximately 1 μm in length and 100 nm in diameter. During fabrication, the ion beam energy was maintained at 10 KeV while the beam current was gradually reduced to 0.1 nA to prevent possible damage and Ga implantation to the bulk of the final pillar structure. Based on the milling parameters used in this study (including the fact that the ion beam was used at a glancing angle) and results reported elsewhere,[15] the damage to the surface layer is expected to be about 3 nm. To further protect the pillars during sample handling and transfer between TEM and SEM stages and shock apparatus, the thickness of the Omniprobe grid post was kept significantly higher (40 μm) than that of the pillars.

A schematic of the laser-shock setup is shown in Fig. 2. In a typical experiment, the Cu grid sample was sandwiched between two 1-mm-thick glass slides such that the axes of the Cu nanopillars (x_2; see Fig. 2 inset) lay sideways parallel to the faces of the glass slides. The top surface of the top glass slide was coated with a 0.5-μm-thick laser-absorbing Al film, which was further constrained from the top by a transparent 20–50 μm thick layer of waterglass. The entire glass slide/TEM grid assembly was mechanically joined using a water-tight tape around sample's edges. DI water was filled between the two glass slides prior to taping which ensured proper coupling and continuity across both glass slide/TEM grid interfaces to allow transmission of the pressure waves across them.

A nominal 8 ns long Nd:YAG laser pulse was focused over 3 mm diameter area on the Al film, which was kept constant in all experiments reported here. Upon absorption of the laser energy, the Al film melts and exfoliates. This process resulted in the launching of a pressure wave σ_{11} (see x_1-x_2 axes in Fig. 2 inset) with a 1–2 ns rise-time and 16–20 ns duration towards the TEM grid sample in manner previously described in Refs. 14 and 16. Because of the DI water, the pressure wave transmits into the TEM grid and

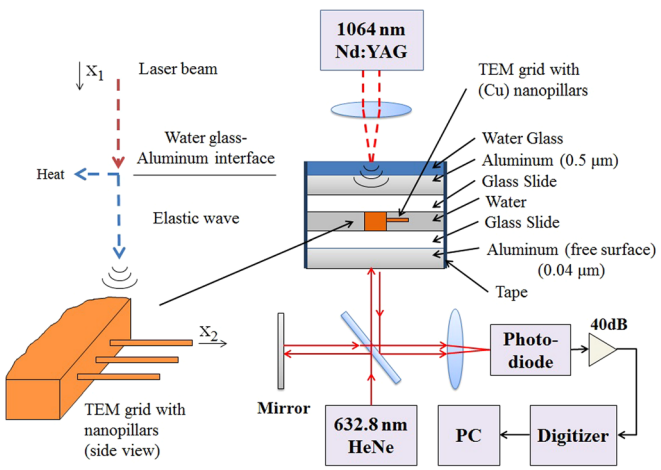

FIG. 2. Experimental setup used to dynamically bend copper nanopillars using laser generated stress waves.

[This article is copyrighted as indicated in the article. Reuse of AIP content is subject to the terms at: http://scitation.aip.org/termsconditions. Downloaded to] IP: 128.97.83.27 On: Fri, 10 Jan 2014 00:16:10

exits through the rear glass slide after transversely loading the Cu nanopillars. The tensile unloading wave from the rear surface of the second glass substrate does not reload the Cu nanopillars as this wave is entirely trapped within the glass plate because the arrival of the first tension separates the DI water/lower glass slide interface as it is under minimal assembly stress.

In order to obtain the background stress-state within the copper sample and to determine the local strain rate of deformation, a state-of-the-art optical interferometer (see Fig. 2), capable of recording fringes with 0.2 ns resolution in the single shot mode, was used to measure the free surface velocity $v(t)$ of the bottom surface of the top glass slide in a separate specimen in which no TEM grid with Cu nanopillars was attached. For this purpose, a 0.1-μm-thick Al film was deposited on the rear surface of the glass slide, which acted as a reflective medium for the interferometric He-Ne laser beam for recording wave-induced surface accelerations and decelerations. The recorded velocity was used to calculate the history of the stress wave $\sigma_{11}(t)$ that was generated in the top glass slide of thickness h and density ρ using the equation

$$\sigma_{11}(t) = \frac{\rho c_o}{2}\left[v\left(t+\frac{h}{c}\right) - v\left(t-\frac{h}{c}\right)\right], \qquad (1)$$

where c_o (= 2289 m/s) is the longitudinal wave speed in glass. Details of interferometer methodology can be found in Refs. 17–19. This initial stress wave was then used as an input to a one-dimensional wave propagation model of a multilayered medium composed of three layers including the two glass slides and the water layer. Details of the model, including its analytical solution, have been presented elsewhere.[17,20] The model provides stress histories at any point, including all interfaces, by fully considering all wave reflections and transmissions. The model did not incorporate the copper layer since the wave travels through the copper pillars in about ~0.02 ns, a time well below the rise time of the shockwave of nearly 5 ns. The model was used to determine the stress history at the middle of the TEM grid, located at 12.5 μm from the top glass slide/water interface. This was taken as the overall stress loading the nanopillars. Of specific interest was to determine the duration of loading on the nanopillars from which the overall strain rate was estimated based on the analysis of bending deformation observed in post-shocked samples from a TEM micrograph. A maximum strain rate $\frac{d\in_{11}}{dt}$ of $2 \times 10^7\,s^{-1}$ is estimated for the present experiments. The exact stress-state inside each pillar, as needed to carry out the MD simulations, was determined using a finite element simulation with the overall stress as an input. In this paper, we report only the strain rate measurements and the background stress-state causing the observed deformations and leave the details of the finite element analysis to another communication where we will report results of the MD simulation.

Each group of pillars were loaded only once at different laser energies. Morphologies and structures of the nanopillars were characterized before and after shock loading using SEM JSM 6700R (JEOL) and a TEM Titan (FEI) operated at 300 kV. Plasma cleaner was used to remove possible contamination of the samples prior to TEM examination. Since the shocked samples were TEM ready, no further preparation was necessary.

III. RESULTS

Fig. 3 shows SEM images of the nanopillars before (a) and after (b)–(e) they were shock loaded at increasing laser energies. Permanent plastic bending in the pillars in the x_1-x_2 plane due to the transverse stress wave σ_{11} is evident even at the lowest laser energy of 250 mJ when compared with the control (straight) sample in (a). The extent of bending and local plastic deformation increased with an increase in the laser energy. The 90° bend in the pillar was caused by the shock wave generated at 450 mJ laser energy. The pillar was completely fractured when shocked at 800 mJ.

To confirm that pillar bending was caused by the shock wave and not from any extraneous effects such as sample handling during TEM examination or sample transfer between SEM and TEM stages, a series of control experiments were performed where pillars were examined under a SEM before and after shock loading, prior to TEM examination. For the control experiment, 4 TEM grids were permanently attached to the SEM specimen-post using carbon tape. The entire post could be easily transferred between the SEM and shock apparatus without removing the sample. Figure 4(b) shows the SEM image of a pre-shocked pillar while Figure 4(c) shows the same pillar bent by the shockwave at 450 mJ. Figure 4(d) shows the image of the same sample in Fig. 4(c) when it was re-shocked by another stress wave at 450 mJ. Damage in Fig. 4(c) and additional damage in

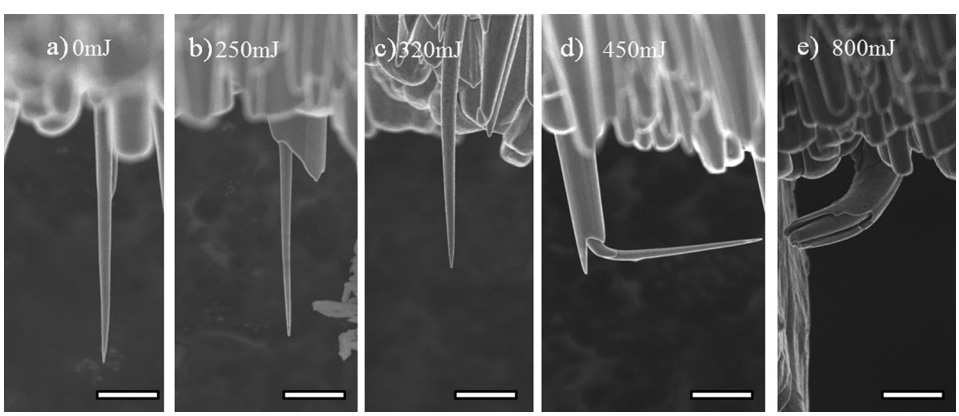

FIG. 3. SEM images of the nanopillars before (a) and after (b)–(e) the treatment by the laser shock wave with different laser energies (indicated on the images). Scale bars in all images are 1 μm.

[This article is copyrighted as indicated in the article. Reuse of AIP content is subject to the terms at: http://scitation.aip.org/termsconditions. Downloaded to] IP: 128.97.83.27 On: Fri, 10 Jan 2014 00:16:10

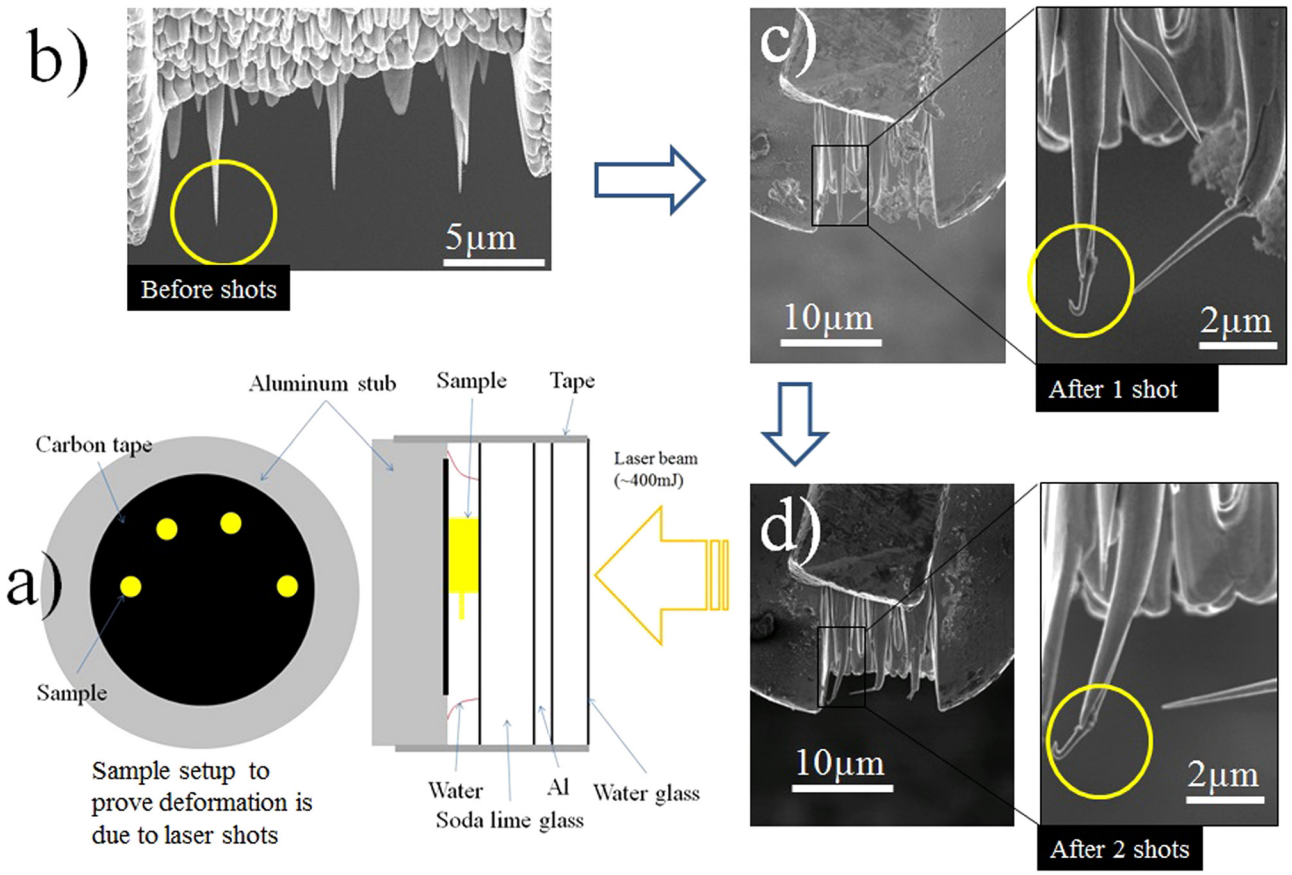

FIG. 4. Control experiments. Bottom-left: Grids are attached to the SEM post using the carbon tape. The next schematic is that of the entire post as located inside the LST apparatus. SEM Images: Clockwise from top left-SEM evaluation of the sample before, after the first, and after the second laser shot, both tested with laser beam energy of 450 mJ.

Fig. 4(d) due to the second shock confirm that bending in the nanopillars can be solely attributed to shockwave loading.

Most pillars were initially single crystals. TEM results are shown in Fig. 5 for one such pillar. Selective area electron diffraction patterns from the tip of the pillar (insets) are consistent with this observation (a) and (b). When this pillar was shocked by a stress wave generated at 320 mJ, it resulted in a slight bending of the pillar (see also Fig. 3(c)). This slight deformation was insufficient to cause any high angle grain boundaries within the single crystal region of the pillar as evident from its diffraction pattern, which shows a single crystal signature (inset in Fig. 5(b)). However, when the pillar was bent 90° by a much higher amplitude shockwave generated at 450 mJ, the single crystal pillar become

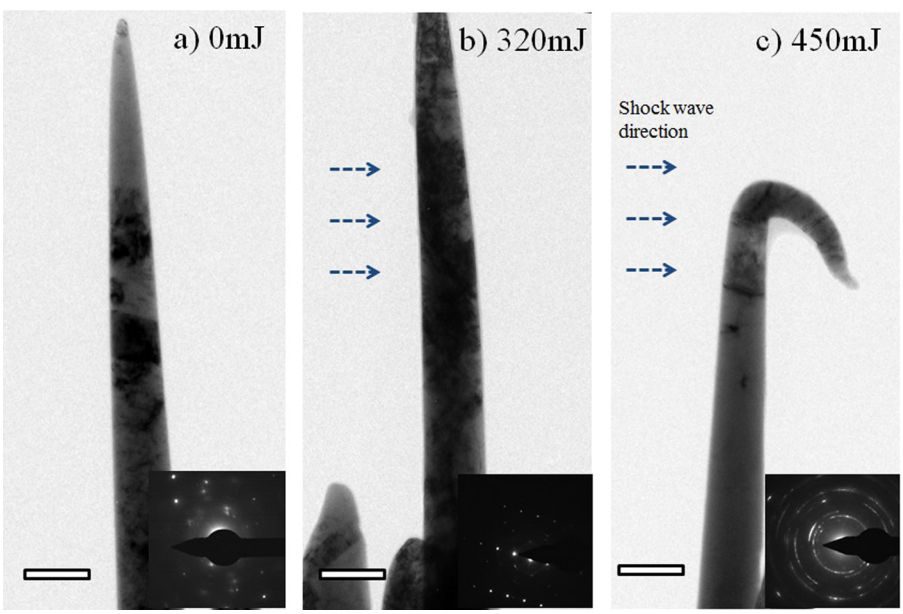

FIG. 5. TEM bright-field images of the nanopillar before (a) and after laser shot at 320 mJ (b) and 450 mJ (c). Insets show corresponding diffraction patterns taken from the tip of the pillar. Scale bars in all images are 200 nm.

[This article is copyrighted as indicated in the article. Reuse of AIP content is subject to the terms at: http://scitation.aip.org/termsconditions. Downloaded to] IP: 128.97.83.27 On: Fri, 10 Jan 2014 00:16:10

polycrystalline as demonstrated by the diffraction pattern in Fig. 5(c).

Figure 6 shows typical TEM images and selected area electron diffraction (SAED) patterns acquired from one such Cu pillar before (a) and (b) and after (c) and (d) it was shocked with a stress wave generated with 400 mJ laser pulse. The TEM image shows straight line suggestive of a twin boundary within the crystal, which was confirmed by indexing of SAED pattern. A few dislocations are also visible in the image. Dark-field image of the pillar obtained using reflection (200) is shown as an inset in Fig. 6(a). The brighter contrast in the image highlights one of the twin crystals, referred to here as the parent crystal. After the shock treatment, we notice the presence of the twin crystal in the tip of the pillar (Fig. 6(c)). However, the twin boundary visible in Fig. 6(a) before laser treatment appears to have changed shape. The SAED pattern in Fig. 6(d) and the dark-field image reveal a change in the microstructure of the pillar after shock treatment. The contrast visible in the dark-field image is due to the presence of a large number of dislocations in the pillar. SAED pattern in Fig. 6(d) is indicative of multiple subgrain boundaries and development of a texture at the nanoscale. It is interesting to note that dislocation nucleation and motion due to laser shock resulted in the deformation of the twin crystals and led to the formation of multiple dislocation subgrains. Such deformation response is not typical in compressed nano-pillars, where the starvation mechanism has been postulated to depopulate pillars from pre-existing dislocations and lead to surface nucleation at high stress values. High resolution TEM (HRTEM) images of the same pillar obtained from the vicinity of the twin boundary are shown in Fig. 7. Fourier transforms (FT) of the HRTEM images (c) and (d) clearly show the presence of new grains.

IV. OVERALL STRESS STATE AND ESTIMATION OF STRAIN RATE

Figure 8(a) shows the raw fringe data from the Michelson displacement interferometer, which was reduced to obtain transient histories of free surface displacement (Fig. 8(b)) and stress σ_{11} (Fig. 8(c)) in the upper glass slide using the procedures described previously.[20] Fig. 9 shows the stress wave profiles obtained at different laser energies using the same interferometric procedures. The recorded stress wave in the upper glass slide was used as an input into a one-dimensional wave propagation model of a three-layer medium composed of the water layer and the two glass slides. The copper layer was not considered in the model because of its extremely small thickness. The wave propagation time through the pillars is about ~0.02 ns, which is well below the rise time of the stress wave of ~5 ns. The governing wave equations were solved analytically in all three domains by satisfying the traction and displacement continuity conditions across each interface. The free surface of the bottom glass slide was kept stress free. Because of the very high strain rate loading, water was modeled as an effective solid with density 1,000 kg/m^3 with a wave speed 1481 m/s. Details of the solutions are provided

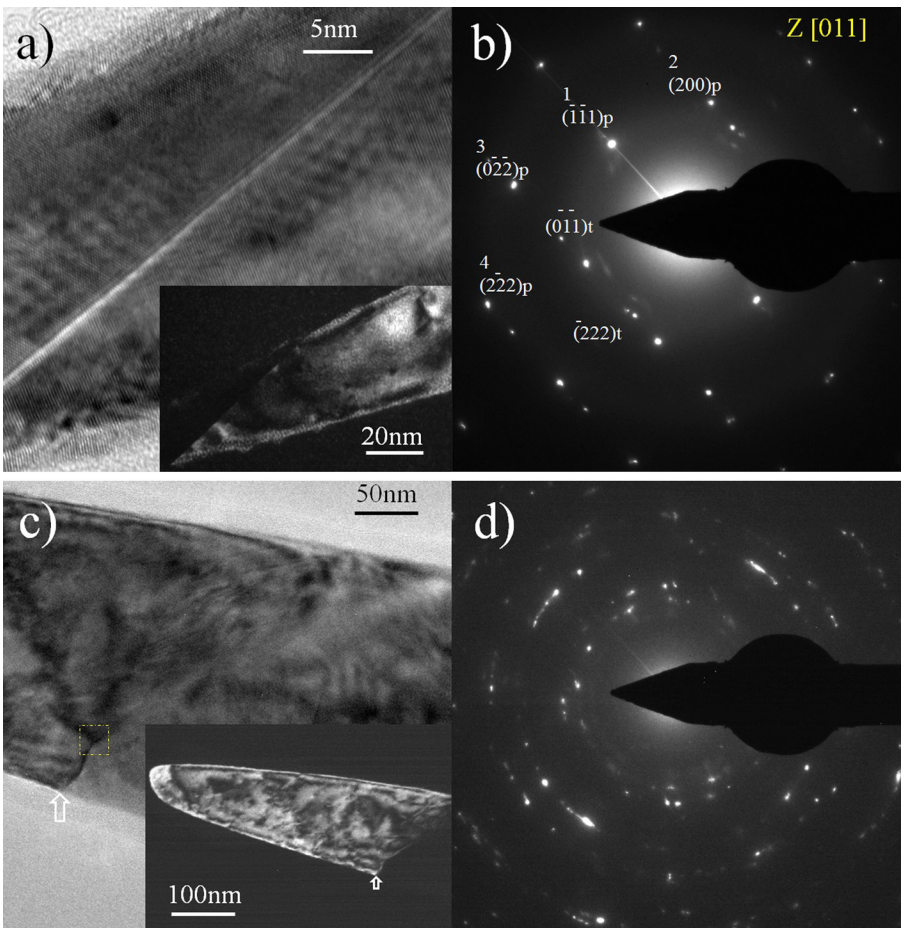

FIG. 6. Bright (a) and (c) and dark (insets) field-images of the area of the pillar in the vicinity of the twin boundary. Corresponding SAED patterns are shown in (b) and (d). Images (a) and (b) show the pillar before the treatment and (c) and (d) after its shock loading at 320 mJ. The parent and twin (rotated) copper planes are designated on image (b) with a p and t subindexes, respectively.

[This article is copyrighted as indicated in the article. Reuse of AIP content is subject to the terms at: http://scitation.aip.org/termsconditions. Downloaded to] IP: 128.97.83.27 On: Fri, 10 Jan 2014 00:16:10

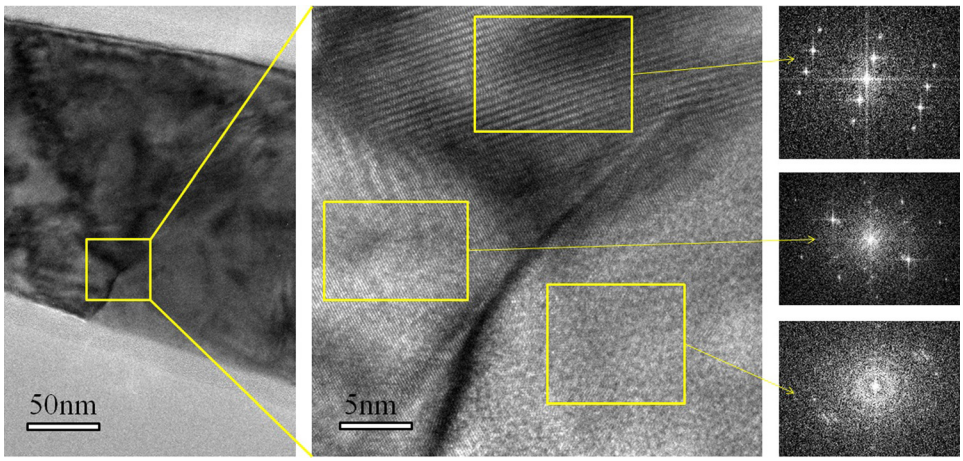

FIG. 7. HRTEM images of the area of the pillar boxed in Figure 6(b). Panel to the right show FFT patterns of different areas boxed in the central panel. Two areas taken above the twin boundary has different orientation.

elsewhere.[17,20] Figure 10 shows the computed σ_{11} stress history for the Cu pillar shown in Fig. 5(a), which was bent by the stress wave generated at 450 mJ of laser energy. The computation was carried out using the stress wave profile corresponding to 450 mJ from Fig. 8(c). The pillar was subjected to a peak σ_{11} stress of 297 MPa. It was also subjected to multiple compressive stress waves that are generated from internal reflections from the two interfaces before the reflected tensile wave from the free surface of the bottom glass slide separates the bottom glass slide/water interface to cut off the loading to the nanopillars. Even though the nanopillar is subjected to these multiple compressive waves, they do not cause any microstructural damage to the pillar as their amplitude is well below 154 MPa, a level that was determined as the threshold to cause microstructural damage. This was determined by loading nanopillars at increasing stress wave amplitudes and examining the resulting microstructures using scanning and transmission electron microscopes. The arrival of the first compressive stress front in Fig. 10 at the Cu nanopillar is approximately ~178 ns, and is exactly the time it takes for the elastic wave to propagate, at the p-wave speed, through the top glass slide and through half the distance of the water layer of 25 μm (pillar location). An impedance mismatch exists between the glass and water layers that only allows for 18% of the initial wave amplitude ($\sigma_{11} = 284$ MPa) to be transmitted. After loading the nanopillars, the wave continues toward the lower glass slide interface where it is reflected back with 82% of its energy and re-loads the pillars 8.45 ns later (half the time to travel the full water layer) with a second amplitude of 233 MPa. Even though the latter reflection is tensile, the overall stress-state is still compressive due to the superposition with the massive incoming compression wave.

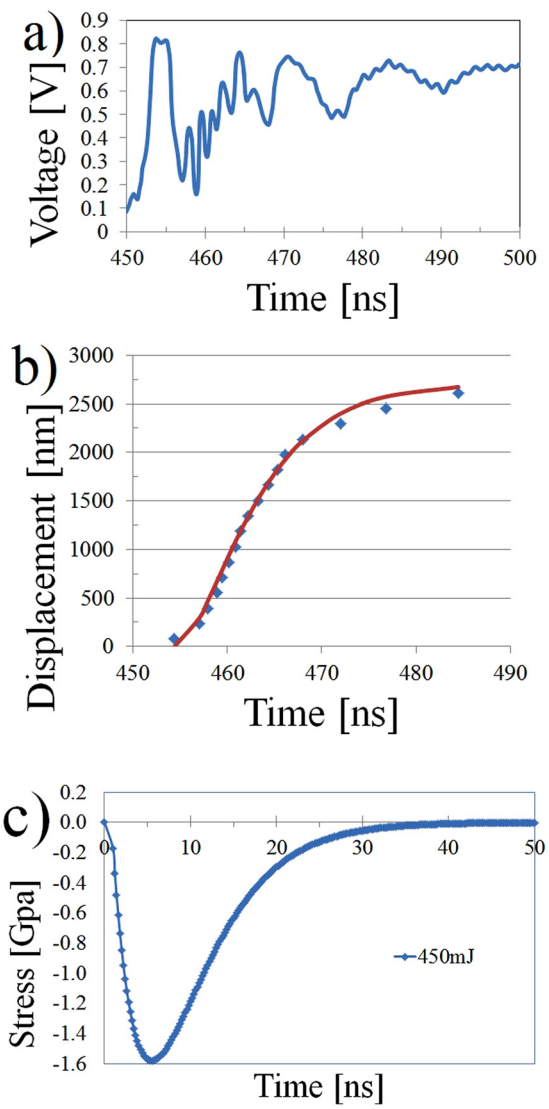

FIG. 8. (a) Raw data from Michelson displacement interferometer corresponding to 450 mJ laser shot. (b) Extracted displacement data and fitted displacement curve. (c) Calculated stress wave profile corresponding to (b).

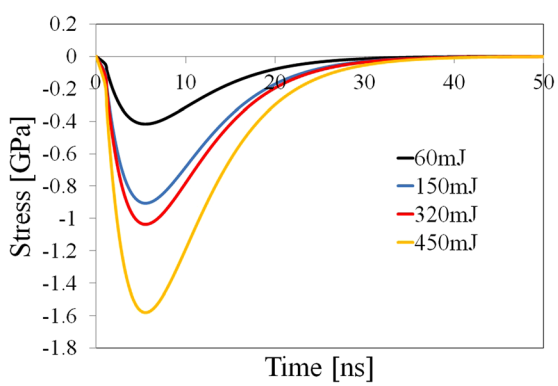

FIG. 9. Measured stress wave profiles at different laser energies.

[This article is copyrighted as indicated in the article. Reuse of AIP content is subject to the terms at: http://scitation.aip.org/termsconditions. Downloaded to] IP: 128.97.83.27 On: Fri, 10 Jan 2014 00:16:10

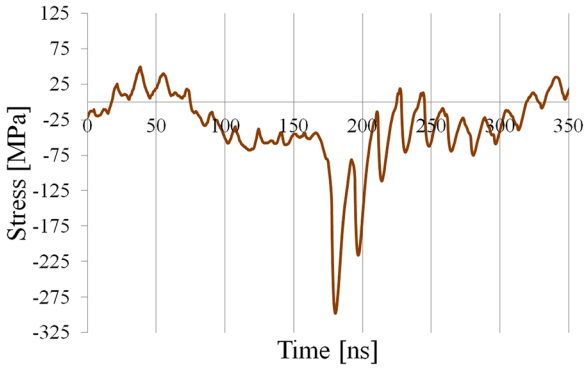

FIG. 10. Calculated σ_{11} stress history at the location of the nanopillar when loaded by a laser-generated stress wave profile shown in Fig. 8(c).

The calculated stress in Fig. 10 represents the overall load but not the local stress within the nanopillar, which requires further finite element simulation. However, the maximum strain rate of deformation can be determined using geometrical considerations. The maximum strain at the convex section of the 90° bent nanopillar can be estimated to be 0.57. This is based on the maximum stretch experienced by the convex fiber of the pillar when it is bent in the x_1-x_2 plane. This strain occurs over the total duration of stress wave loading of 22.5 ns, which was taken from Fig. 10 as the length of the intercept made by intersection of the 154 MPa (below which no damage is caused in the pillars) line with the two stress peaks. The average strain rate $\frac{d\epsilon_{11}}{dt}$ is thus $2.5 \times 10^7 s^{-1}$, assuming that the bending was caused by both stress peaks. This is the lowest estimate. The highest estimate will be $2.8 \times 10^8 s^{-1}$ if the entire strain occurs during the first stress spike with a rise-time of about 2 ns.

V. DISCUSSION

An experimental study of bending cantilevered single crystal Cu nanopillars of several hundred nanometers in diameter and length at ultrahigh strain rate is presented. The deformation is induced by laser-generated stress waves resulting in local strain rates exceeding $10^7 s^{-1}$. At a nominal σ_{11} stress value of 297 MPa, TEM examination along with the SAED study revealed that the single crystal within the unshocked Cu pillars were converted into multiple dislocation subgrains. The classical picture of the accommodation of bending by arrays of geometrically necessary dislocations appears not to be followed in the deformation pattern of bent nano-pillars with shock waves. Rather, small dislocation loops are seen to nucleate from the abundant surface areas of the pillars and organize themselves into nano-scale dislocation subgrains. The rotation associated with the presence of dislocation subgrains is postulated to be the accommodation mechanism of nanopillar bending under shock loading conditions. The formation of nanoscale subgrains that accommodate bending rotation is the result of dislocation emission from the surface of the pillars under shock loading, as evidenced in Fig. 6(c). This level of nominal axial stress (the local stress, enhanced by pillar bending, is likely to be below one GPa) is far below the stress levels known for the homogeneous nucleation of dislocations in bulk Cu single crystals, in the range of 1–3 GPa in shear. Considering the Schmidt factor, the Critical Resolved Shear Stress (CRSS) is likely to be an order of magnitude smaller that values reported in the literature for the homogeneous nucleation of dislocations from the bulk or even at a surface step. The low experimental values are however consistent with our current MD studies, which show that the stress to nucleate and propagate Shockley partial dislocations inside a single crystal nanofilm shocked in the [100] direction was drastically reduced to an axial σ_{11} stress of only 1–2 GPa for a 60 nm diameter single crystal nanopillar shocked along the [100] and [111] directions that were aligned with the x_1 axis. Unlike the nanofilm case, where dislocations were nucleated in the interior, all dislocations (both partials in the [100] and [111] cases, and perfect (only in the [111] case)) in the nanopillars nucleated at the free surface. MD simulations were performed with the LAMMPS Software, with the Mishin EAM interatomic potential for copper. Typical simulation times were 30–60 picoseconds, with time steps of 1 femtosecond. All simulations began with a ramped thermal equilibration using an NPT ensemble to 300 K. Nanofilms were given periodic boundary conditions along the directions transverse to loading, with sizes $25 \times 25 \times 100$ nm^3, containing 5.5 million atoms. Nanopillars were 60 nm diameter cylinders with free boundaries in all directions, containing about 14 million atoms. The piston speed in the MD simulations is between 100–1000 m/s, and the pillar length is typically 100 nm. Thus, the average strain rate is 10^9–$10^{10} s^{-1}$. Details of the simulations will be presented in a forthcoming publication.[21]

There is no prior work available on Cu single crystal pillars of such small dimensions at ultrahigh strain rates to compare our results but comparison with related mechanisms can be done. For example, nucleation of twins was observed in copper samples with 40 μm grain size when the sample was shock loaded at 20 GPa.[22] The stress dropped to 15 GPa as the grain size was increased to 200 μm. Other works[23] have reported a threshold twining stress of 25 GPa in the [011] orientation and between 40 and 60 GPa in the [134] orientation. These stresses are well in excess of what is reported here.

It has been shown before that twin boundaries can migrate under strain in pure copper.[24,25] This occurs via Shockley partial dislocation emissions at the twin boundary/grain boundary (GB) intersections. This mechanism is however unlikely to explain the present observations as the Cu columns were single crystals to begin with, with very few twins. There is nevertheless evidence in our experiments that twins migrated in shocked pillars at fairly low stress levels. Perhaps the very large surface to volume ratio in our samples allows this to happen as it so does for nucleating dislocations from pillar's free surfaces. More experiments and MD simulations are in progress to further elucidate this mechanism. The relatively low values of the transverse stress amplitude that caused the substantial bending of copper nanopillars is consistent with a mechanism of intense surface nucleation of dislocation loops, their interaction with twin boundaries, and their self-organization in dislocation sub-boundaries. Such an organization seems to be the accommodating mechanism of the large bending strain in shocked nanopillars, as contrasted with the classic mechanism of geometrically necessary arrays of dislocations. It appears that the relative

[This article is copyrighted as indicated in the article. Reuse of AIP content is subject to the terms at: http://scitation.aip.org/termsconditions. Downloaded to] IP: 128.97.83.27 On: Fri, 10 Jan 2014 00:16:10

abundance of surfaces in nanopillars facilitates nucleation and coherent assembly of dislocation; and as a consequence, lattice rotation can accommodate large bending strains.

ACKNOWLEDGMENTS

The authors thank the NSF for the support through the Grant No. 1024353. H.A.C. gratefully acknowledges support from Colciencias-Universidad de Antioquia (Colombia) for the permission to work on this project.

[1]G. R. Johnson, J. M. Hoegfeldt, U. S. Lindholm, and A. Nagy, J. Eng. Mater. Technol. **105**(1), 42–47 (1983).
[2]F. J. Zerilli and R. W. Armstrong, Acta. Metall. Mater. **40**(8), 1803–1808 (1992).
[3]P. S. Follansbee and U. F. Kocks, Acta. Metall. Mater. **36**(1), 81–93 (1988).
[4]K. G. Hoge and A. K. Mukherjee, J. Mater. Sci. **12**(8), 1666–1672 (1977).
[5]D. J. Steinberg and C. M. Lund, J. Appl. Phys. **65**(4), 1528–1533 (1989).
[6]D. J. Steinberg, S. G. Cochran, and M. W. Guinan, J. Appl. Phys. **51**(3), 1498–1504 (1980).
[7]D. L. Preston, D. L. Tonks, and D. C. Wallace, J. Appl. Phys. **93**(1), 211–220 (2003).
[8]M. Kiritani, J. Mater. Sci. Eng. **350**(1–2), 63–69 (2003).
[9]M. Kiritani, K. Yasunaga, Y. Matsukawa, and M. Komatsu, "Plastic deformation of thin metal foils without dislocations and formation of point defects and point defect clusters," in *Proceedings of Materials Research Society Spring Meeting, San Francisco, CA* (2001).
[10]B. A. Remington *et al.*, Mater. Sci. Tech. Ser. **22**(4), 474–488 (2006).
[11]L. Li and N. M. Ghoniem, Phys. Rev. B **79**(7), 075444 (2009).
[12]E. M. Bringa *et al.*, Science **309**(5742), 1838–1841 (2005).
[13]G. Youssef, R. Crum, S. V. Prikhodko, D. Seif, G. Po, N. Ghoniem, S. Kodambaka, and V. Gupta, J. Appl. Phys. **113**, 084309 (2013).
[14]J. Yuan and V. Gupta, J. Appl. Phys. **74**(4), 2388–2404 (1993).
[15]S. Shim, H. Bei, M. K. Miller, G. M. Pharr, and E. P. George, Acta Mater. **57**, 503–510 (2009).
[16]V. Gupta, J. Yuan, and A. N. Pronin, J. Adhesion Sci. Technol. **8**(6), 713–747 (1994).
[17]A. N. Pronin and V. Gupta, J. Mech. Phys. Solids **46**(3), 389–410 (1998).
[18]L. M. Barker and R. F. Hollenbach, J. Appl. Phys. **41**(10), 4208–4226 (1970).
[19]R. J. Clifton, J. Appl. Phys. **41**(13), 5335–5338 (1970).
[20]V. Gupta, A. S. Argon, D. M. Parks, and J. A. Cornie, J. Mech. Phys. Solids **40**(1), 141–180 (1992).
[21]D. Seif, G. Po, R. Crum, S. V. Prikhodko, S. Kodambaka, V. Gupta, and N. Ghoniem, "Molecular dynamics simulations of shock-loaded copper nano-films and nano-pillars," J. Appl. Phys. (unpublished).
[22]J. Petit and J. L. Dequiedt, Mech. Mater. **38**(3), 173–185 (2006).
[23]M. S. Schneider, B. Kad, D. H. Kalantar, B. A. Remington, E. Kenik, H. Jarmakani, and M. A. Meyers, Int. J. Impact Eng. **32**, 473–507 (2005).
[24]D. P. Field, B. W. True, T. M. Lillo, and J. E. Flinn, Mater. Sci. Eng. A **372**(1–2), 173–179 (2004).
[25]Y. B. Wang, M. L. Sui, and E. Ma, Philos. Mag. Lett. **87**(12), 935–942 (2007).

[This article is copyrighted as indicated in the article. Reuse of AIP content is subject to the terms at: http://scitation.aip.org/termsconditions. Downloaded to] IP: 128.97.83.27 On: Fri, 10 Jan 2014 00:16:10

View publication stats